J. Phys. B: At. Mol. Opt. Phys. **29** (1996) 5527–5542. Printed in the UK

Electron impact excitation of autoionizing levels of Kr and Xe between the $^2P_{3/2}$ and $^2P_{1/2}$ ionic limits

Lance R LeClair† and Sandor Trajmar‡

Jet Propulsion Laboratory, California Institute of Technology, Pasadena, CA 91109, USA

Received 9 July 1996

Abstract. We have observed electrons ejected from autoionizing levels which lie between the $^2P_{3/2}$ and $^2P_{1/2}$ ionic limits for Kr and Xe. Kinetic energy spectra of the ejected electrons were obtained following electron-impact excitation of the target gases by using time-of-flight spectroscopy in a crossed-beam experiment. Spectral features which correspond to electrons ejected from both odd and even parity autoionizing levels have been identified. Some of the features have kinetic energies of just over 0.1 eV and have been resolved for the first time in an electron-impact experiment. The most intense features at low electron-impact energies come from optically forbidden $n\mathrm{p}'$ and $n\mathrm{d}'$ terms. It was possible to estimate the integral cross section for autoionization by comparing the intensity of the elastically scattered electrons with the intensity of the autoionizing features. For Xe, autoionization from the levels which lie between the ionic limits appears to account for about 67% and 7.6% of the electron-impact ionization cross section at impact energies of 14 and 24 eV, respectively; while for Kr, the fractions are 20% and 2.7% at 16 and 26 eV.

1. Introduction

Autoionization is a fascinating phenomenon which has attracted considerable experimental and theoretical interest. The autoionizing levels of heavy rare gases which lie between the $^2P_{3/2}$ and $^2P_{1/2}$ ionic limits (hereafter referred to as the low AI levels) have been the subject of many photon-impact studies in recent years. These efforts have utilized single-photon excitation from the ground state (e.g. Maeda *et al* 1993) and multiphoton excitation from the ground state or metastable levels (e.g. Wang and Knight 1986, Klar *et al* 1992, Koeckhoven *et al* 1994, 1995) in order to obtain energies, lineshapes, lifetimes, quantum defects, and photoabsorption cross sections for many of the low AI levels. The use of multiphoton techniques has enabled many of the otherwise optically forbidden low AI levels to be reached.

Even though electron-impact excitation of the low AI levels can be a significant ionization channel, such studies have attracted much less attention, possibly because of experimental difficulties. Electron-impact excitation of an AI level from the ground state proceeds as follows,

$$\mathrm{e}(E_0) + \mathrm{X} \rightarrow \mathrm{e}(E_r) + \mathrm{X}^*(\Delta E)$$
$$\mathrm{X}^*(\Delta E) \rightarrow \mathrm{X}^+ + \mathrm{e}(E_{ej}),$$

† National Research Council Resident Research Associate. E-mail address: LANCER@SCN1.JPL.NASA.GOV
‡ E-mail address: SANDOR@SCN1.JPL.NASA.GOV

0953-4075/96/225527+16$19.50 © 1996 IOP Publishing Ltd

where $E_0 = E_r + \Delta E$, E_0 is the kinetic energy of the incident electron, E_r is the residual energy of the scattered electron, and ΔE is the excitation energy of the autoionizing level (that is, the energy lost by the incident electron). Note that dipole selection rules can be thrown out since electron exchange can take place if E_0 is low enough. Since X^* lies in the ionization continuum, it can autoionize by ejecting a second electron with energy $E_{ej} = \Delta E - E_i$, where E_i is the ionization energy of X. One additional complication arises from the fact that autoionizing levels are very short lived (from femto- to picosecond lifetimes). If E_r is very small (several meV) the scattered electron may still be in the neighbourhood of the excited target when the second electron is ejected (depending on the lifetime) and a post-collision interaction (PCI) between the two electrons will occur.

Electron-impact excitation of autoionizing levels can be studied by detecting the product ion, the scattered electron, or the ejected electron; either separately, or in coincidence. The only previous electron-impact studies of the low AI levels of rare gases have been those of Marmet and Proulx (1990), and Hammond *et al* (1988). Marmet and Proulx observed the low AI levels as small perturbations to the total Xe^+ production curve, measured as a function of E_0. Hammond *et al* have observed the low AI levels by utilizing threshold electron-energy loss spectroscopy (EELS). In their case, only electrons with $E_r < 20$ meV were collected as a function of E_0. The ensuing results were particularly useful for a study of PCI effects (Read and Hammond, 1988). There are other electron impact studies of AI levels in rare gases (e.g. see Comer 1992, Baxter *et al* 1983), but those were concerned with levels which produced ejected electrons with energies greater than several eV. This was probably because electrons with such kinetic energies are easily analysed with conventional electron-energy spectrometers employing electrostatic dispersive elements. Electrons with kinetic energies of a few tenths of an eV are difficult to observe with a conventional electrostatic spectrometer because low-energy electrons are more susceptible to the aberrations and surface conditions of the lenses which are employed to collect the electrons and guide them through the dispersive elements of the spectrometer.

Recently, we have constructed a time-of-flight (TOF) electron spectrometer which is free of focusing and energy-dispersing electric and magnetic fields. This spectrometer was utilized to measure ratios between inelastically and elastically scattered electrons (from gaseous targets) which are free from the instrumental effects encountered with conventional electrostatic spectrometers. These ratios, in turn, can serve as secondary standards for normalizing inelastic differential cross sections obtained from measurements made with conventional electrostatic spectrometers (LeClair and Trajmar, 1996). During our work with rare gases, we noticed the appearance of sharp structures at very long flight times which were due to electrons ejected from the low AI levels. We studied the ejected electron spectra obtained from Kr and Xe and the results of this short investigation are presented below.

2. Apparatus and method

A brief description of the apparatus will be given only, since a detailed description has already been published (LeClair *et al* 1996). Essentially, the apparatus consisted of a mutually orthogonal electron beam, gas beam, and drift tube. These items were placed in a magnetically shielded (< 2 mgauss) vacuum chamber and baked at 150 °C to maintain clean surfaces.

We used a simple electron gun which is capable of producing a highly collimated electron beam of up to 220 nA in the DC mode, from 2 to several hundred eV impact energies. When operated in the pulsed mode, the gun typically produced Gaussian pulses

with widths of several nanoseconds, depending on E_0. We calibrated E_0 by observing the threshold of metastable production for each target gas with a neutral metastable detector. There were no energy-dispersing elements in the gun, so the energy width of the electron beam was about 0.6 eV (FWHM), which is typical of thermionic sources.

The drift tube was constructed out of sheet molybdenum and had two apertures to define a view cone with an apex of 6°. The end of the drift tube was terminated with a grid, followed by a post-acceleration voltage of 450 V onto a stack of 40 mm diameter multi-channel plate electron multipliers. The field-free drift distance for scattered electrons was 21.6 cm, giving an electron TOF, t (ns), of

$$t = 364/\sqrt{E}, \tag{1}$$

where E is the kinetic energy of the electrons in eV. The kinetic energy resolution for ejected electrons is predominantly given by

$$\delta E = 2E\delta t/t \tag{2}$$

where δt represents the temporal width of the incident electron pulse. Thus the energy resolution improves for lower kinetic energies.

TOF spectra were acquired by using a time-to-amplitude convertor (TAC) in conjunction with a pulse-height analyser which operated under the control of a personal computer. The time scale was calibrated with a high-precision digital delay generator. The pulse rate of the electron gun was 100 kHz.

To aid interpretation of features in the TOF spectra, it is convenient to convert them to kinetic energy spectra by a change of variable. That is, if $F(t)$ represents a TOF spectrum, then its kinetic energy spectrum, $F(E)$, is given by

$$F(E) \sim F(t)t^3. \tag{3}$$

One must exercise caution when interpreting features in the kinetic energy spectrum since the t^3 factor in (3) greatly exaggerates noise at long flight times. We applied Gram's method of smoothing to the spectra to reduce the noise (Hildebrand 1987). Also, careful attention must be paid to background subtraction before the transform is done. We used the background in our TOF spectrum which occurred past 1800 ns. The count rate during data acquisition was less than 500 cps, so there was no tilting of the background due to TAC pile-up. The accuracy of the kinetic energy scale depends on the linearity of TAC and the location of the $t = 0$ mark in our TOF spectra. The linearity was checked with a precision digital delay generator, and amounted to a ± 1 ns deviation over 1000 ns. The $t = 0$ mark was located with respect to the maximum of the elastic scattering feature present in each TOF spectrum and calculated by using equation (1) and the calibrated electron-impact energy. This was accurate to within ± 2 ns. Thus the accuracy of the kinetic energy scale for a feature at 540 ns (see figure 2) is about ± 4 meV (from equation (2)), and this improves with increasing TOF.

3. Results and discussion

A TOF spectrum resulting from electron impact on Xe is shown in figure 1. The prominent features due to elastic and inelastic scattering, and the autoionizing features are labelled in the figure. Note that for every ejected electron feature in figure 1, there must be an inelastic feature corresponding to the scattered electron. Such features are not resolved in our TOF spectra because the temporal width for inelastic features depends on the electron pulse width and the energy distribution of the incident electron beam (0.6 eV). However, the temporal

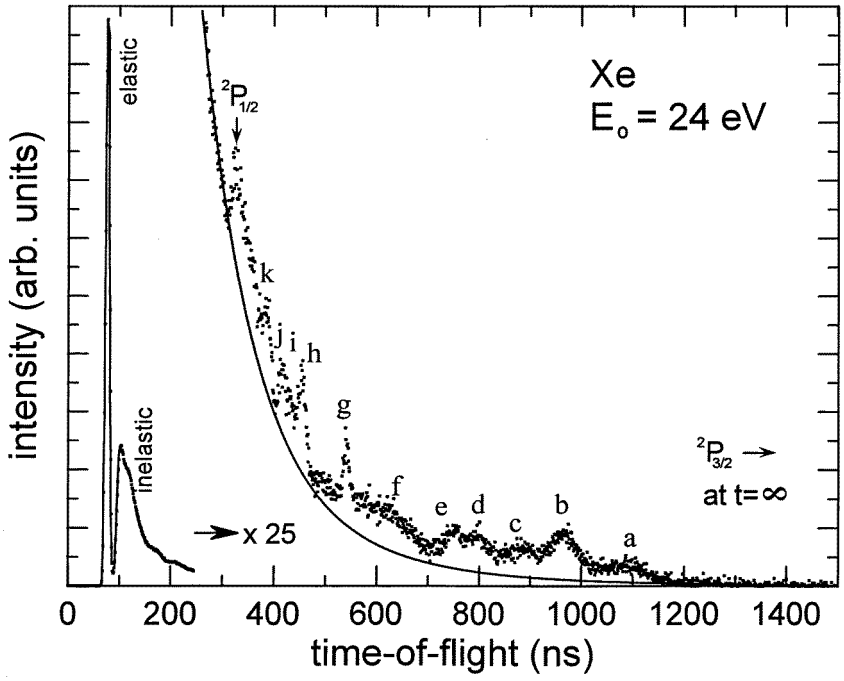

Figure 1. Time-of-flight spectrum obtained from Xe at $E_0 = 24$ eV, $\theta = 90°$. The elastic and inelastic scattering features are below 250 ns. Above 250 ns a magnification factor of 25 has been applied. The features which are due to electrons ejected from autoionizing levels of Xe are labelled a–k. The full curve above 250 ns represents a double exponential fit to the background caused by electrons ejected from the continuum above the $^2P_{3/2}$ ionic state of Xe^+ (see text for details). The positions of electrons ejected at both ionic limits are shown.

width of an ejected electron feature is determined by the duration of the incident electron pulse and the natural lifetime of the AI level responsible for that feature. In the case where an AI level has a narrow energy width (but with a short lifetime compared with the incident pulse) then the width of the AI feature in the TOF spectrum is approximately equal to the duration of the incident pulse. By inspection of feature g in figure 4 it was deduced that the incident pulse width was about 10 ns since the lifetime of the associated level (Xe $8s'[\frac{1}{2}]1$) is about 250 fs (Wang and Knight 1986). This gives an instrumental energy width for that feature of about 20 meV (the natural width is about 2.6 meV). We would like to point out that we did find some small features in the TOF spectra caused by reflection of the incident electron pulse off some of the structures in the vacuum chamber. However, these 'echo' features occurred much earlier in time than the autoionization features. Moreover, they changed shape and decreased in flight time with increasing electron impact energy. The autoionization features occurred at the same TOF regardless of impact energy, as long as E_0 exceeded a characteristic threshold value.

Singly excited levels of heavy rare gases are characterized best by the jl coupling scheme, in which the orbital angular momentum l of the excited electron is strongly coupled to the angular momentum j of the ion core, forming a resultant angular momentum K. K is then weakly coupled to the electron spin s, giving total angular momentum J. The core levels are $np^5\,{}^2P_{1/2}$ and ${}^2P_{3/2}$ (with inverted fine structure), giving $j = \frac{1}{2}, \frac{3}{2}$. Notation is $nl[K]J$, with a prime (′) on l indicating $j = \frac{1}{2}$.

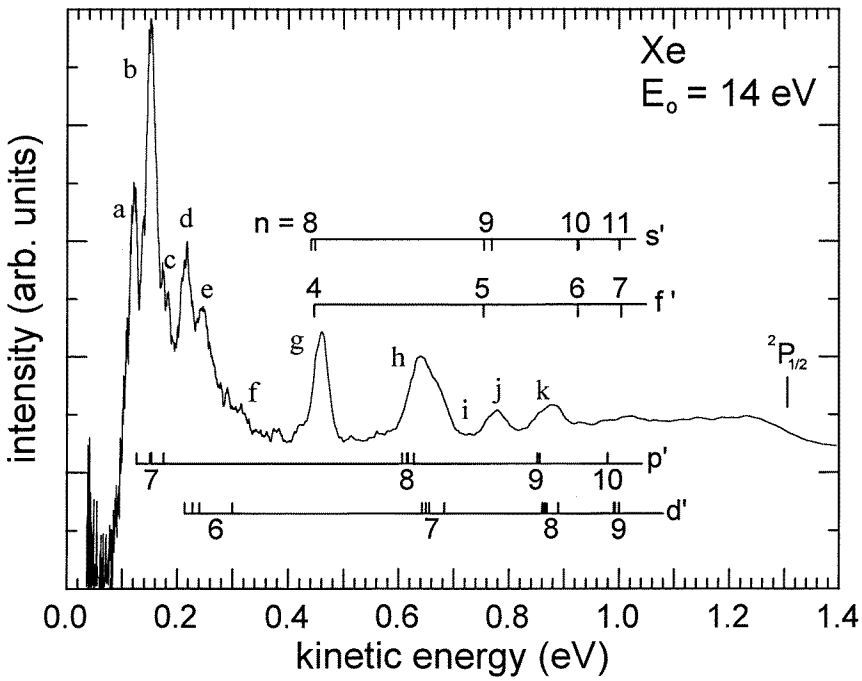

Figure 2. Kinetic energy spectrum of electrons ejected from Xe for $E_0 = 14$ eV. The energies of the s′, p′, d′, and f′ autoionizing series and their fine-structure components are shown for several principal quantum numbers. The exact values of these energies are listed in table 1. The $^2P_{1/2}$ series limit is also shown. The features have been labelled a–k, and correspond to the features with the same labels as in figure 1.

3.1. Xe

The results from Xe will be discussed first since most of the present work was done on it because of its larger autoionization cross section. Kinetic energy transforms of TOF spectra obtained from Xe for electron impact energies of $E_0 = 14.0$, 24.0, and 300 eV are shown in figures 2, 3, and 4, respectively. The features due to electrons ejected from autoionizing levels are labelled a–k, in correspondence with figure 1; and there is a feature l, which appears in figure 4 only. Identification of the levels responsible for features a–l are indicated in table 1, which lists the some of the superexcited levels of Xe between the ionic limits and their corresponding excitation energies. The ejected electron kinetic energy spectra of figures 2 and 3 were acquired using an electron beam of 10 nA (the current was measured in the DC mode) and each took 48 h to acquire. It was much quicker to acquire spectra at higher beam current (figure 4 was acquired in 8 h at 200 nA current), but we found that the positions of the features shifted somewhat to higher kinetic energies (from their spectroscopic values) with increasing electron beam current. We also observed that the shift was not exactly the same for each feature. We are unsure of the reason for the shift, but believe that it is a complex interplay of space charge and surface conditions in the interaction region which are affected by electron beam current. We studied the current-dependent shift only for Xe and only at 14 eV electron impact energy. Time did not permit us to study it at other energies and for Kr.

One obvious observation of figures 2, 3, and 4 is the change in structure with electron

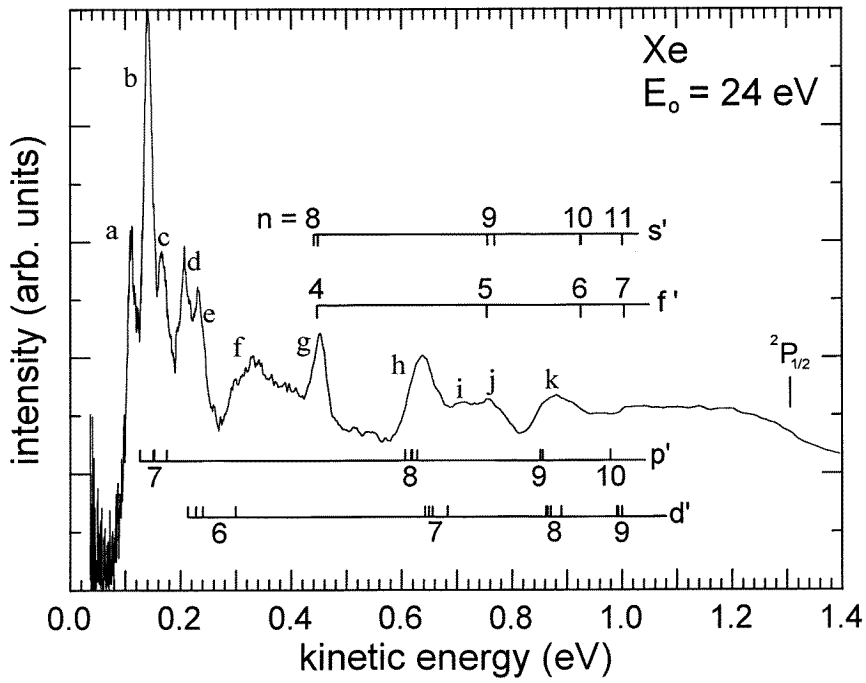

Figure 3. Same as in figure 2, but for $E_0 = 24$ eV.

impact energy. This arises from the well known behaviour of electron impact excitation cross sections for optically forbidden and optically allowed transitions. Electron impact excitation cross sections for levels accessible by optically forbidden transitions peak rapidly within a few eV of threshold and fall off nearly as rapidly. Features a–e and h behave this way, being prominent in figures 2 and 3, but absent from figure 4. Conversely, cross sections for optically allowed transitions gradually increase to reach a maximum which may be dozens of eV above threshold, and then fall off, usually more gradually than the rise to the maximum. Examples here are features f and g which belong to the $n\mathrm{d}'[\frac{3}{2}]1$ and $n\mathrm{s}'[\frac{1}{2}]1$ Rydberg series and are optically accessible from the ground state. Features from these two series are the only ones present in figure 4 ($E_0 = 300$ eV). Note that in figure 4 the s′ series members with $n > 8$ appear as shoulders to the d′ series since the resolution gets worse for higher ejected energies, see equation (2). The resemblance between the ejected electron energy spectrum of figure 4 and photoabsorption spectra of the $n\mathrm{d}'[\frac{3}{2}]1$ and $n\mathrm{s}'[\frac{1}{2}]1$ series of the heavy rare gases (Maeda *et al* 1993) is remarkable, even reproducing the asymmetric Beutler–Fano profile of the $n\mathrm{d}'[\frac{3}{2}]1$ levels. This is yet another example of how electron collisions mimic photon collisions at high energies (Inokuti 1971).

Features a, b, and c originate from the $7\mathrm{p}'[\frac{3}{2}]1$, the unresolved $7\mathrm{p}'[\frac{1}{2}]1$ plus $7\mathrm{p}'[\frac{3}{2}]2$, and the $7\mathrm{p}'[\frac{1}{2}]0$ autoionizing levels of Xe, respectively. They are very prominent, as are the higher members of $n\mathrm{p}'$ series, at low electron impact energies. The excitation energies of these levels have been measured accurately (Grandin and Husson 1981, Koeckhoven *et al* 1995). Feature c may appear to be indiscernible from noise in figure 2, but it is real; it could be seen more clearly by increasing the electron current. Features a, b, and c did not shift any noticeable amount as a function of current up to 100 nA, but by 200 nA it was about 20 meV. Their positions match the spectroscopic values in the $E_0 = 14$ eV spectrum

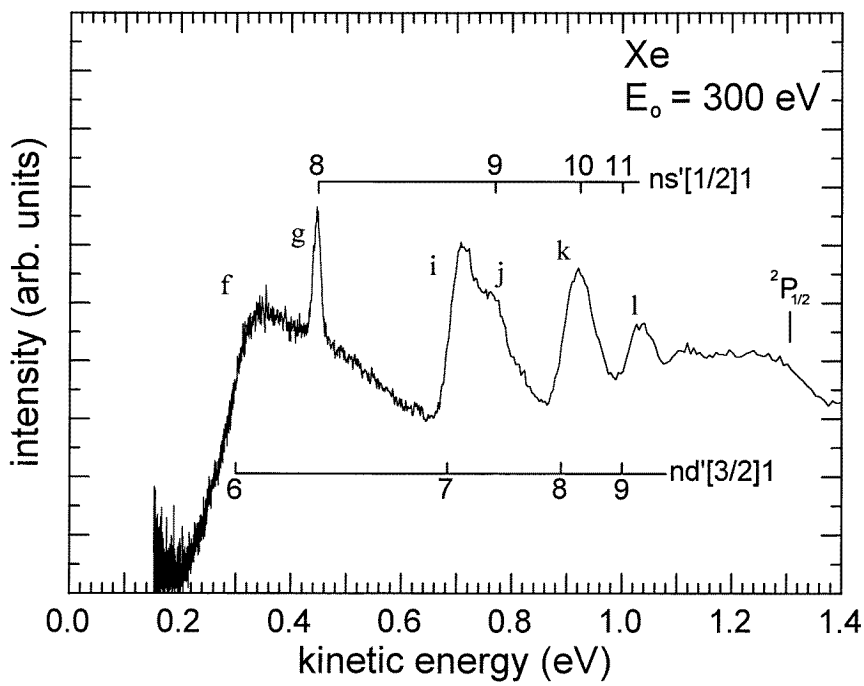

Figure 4. Same as in figure 2, but $E_0 = 300$ eV and only the optically allowed levels are shown. This spectra was taken using a high electron beam current of 220 nA, and consequently was shifted by about 100 meV. The kinetic energy scale has been adjusted so that the 8s′[$\frac{1}{2}$]1 feature appears where it should be, at $E_{ej} = 0.445$ eV, but there remains a slight mismatch between the features and their spectroscopic energies further to the right (see text for details).

(figure 2) but their positions are shifted by about 10–20 meV below their spectroscopic values at $E_0 = 24$ eV (figure 3). We attribute this to slowly building surface patch fields within the drift tube, since figure 3 was acquired after figure 2. Those patch fields probably account for the fairly sharp cut-off of electrons with energies below 0.1 eV in the kinetic energy spectra. As surface patch fields gradually grew worse with time, autoionizing features shifted to lower kinetic energies, and the slowest features would disappear from the spectra.

Features d and e are probably from two of the 6d′[$\frac{5}{2}$]2, 6d′[$\frac{3}{2}$]2, and the 6d′[$\frac{5}{2}$]3 AI levels, with the third being unresolved or absent. We could find no spectroscopic measurements for the excitation energy of these levels. Instead we used the quantum defect for the nd′[$\frac{5}{2}$]3, $n = 8$–40 levels measured by Koeckhoven *et al* (1994), and interpolated with the quantum defect for the $n = 5$ level (Moore 1957). There was practically no change in the quantum defect from $n = 5$ to $n = 8$, so we estimate our calculated energy is close to within 0.01 eV. We calculated the energies of other AI levels in similar fashion, and these have been denoted by an asterix in table 1. A kinetic energy shift of up to 40 meV at 220 nA was observed for these features.

Feature f, as we mentioned above, arises from the 6d′[$\frac{3}{2}$]1 level. Feature f is mostly absent from figure 2, apparent in figure 3, and very strong in figure 4; typical for electron impact excitation of levels which are accessible by optically allowed transitions. The enormous width of feature f (relative to the others) comes from its extremely short lifetime, about 27 fs (Maeda *et al* 1993). The maximum of our feature is slightly higher than the measured spectroscopic value (Maeda *et al* 1993), and this may be due to PCI since the

Table 1. Partial list of Xe autoionizing levels which lie between the $^2P_{3/2}$ and $^2P_{1/2}$ ionic limits and their spectroscopic energies (first column). Also shown are the ejected electron kinetic energies, the features that they correspond to in figure 3, the energies of those features measured by TOF, the intensity ratio of those features with respect to elastic scattering, and their integral cross sections at $E_0 = 14$ and 24 eV. The ionization potentials used for $Xe^+[^2P_{3/2}]$ and $Xe^+[^2P_{1/2}]$ were 12.130 eV (Grandin and Husson 1981) and 13.436 eV, respectively (Wang and Knight 1986). The spectroscopic energies for the table came from the aforementioned references, Maeda *et al* (1993), and Koeckhoven *et al* (1994, 1995). Note that the spectroscopic energies were given in units of cm^{-1} with much more precision than required for this work. They were converted to eV using 1 eV = 8065.541 cm^{-1}, and rounded to five significant figures. The energies denoted by an asterix were obtained by interpolating quantum defects (see text). The J values in parentheses indicate that no measurement is available for that level.

E (eV)	Level $n\ell'[K]J$	Ejected energy E_{ej} (eV)	TOF feature	TOF energy E_{ej} (eV)	R (%) 14 eV	R (%) 24 eV	σ ($\times 10^{-18}$ cm^2) 14 eV	σ ($\times 10^{-18}$ cm^2) 24 eV
12.257	$7p'[\frac{3}{2}]1$	0.127	a	0.110	0.34	0.49	2.0	1.2
12.281	$7p'[\frac{1}{2}]1$	0.151	b	0.150	0.54	1.04	3.1	2.5
12.283	$7p'[\frac{3}{2}]2$	0.153						
12.304	$7p'[\frac{1}{2}]0$	0.174	c	0.170	0.20	0.61	1.2	1.5
12.342*	$6d'[\frac{5}{2}]2$	0.212	d, e	0.210	0.68	1.14	4.0	2.7
12.355*	$6d'[\frac{3}{2}]2$	0.225						
12.369*	$6d'[\frac{5}{2}]3$	0.239		0.245				
12.431	$6d'[\frac{3}{2}]1$	0.301	f	0.330	—	2.00	—	4.8
12.570*	$8s'[\frac{1}{2}]0$	0.440	g	0.450	0.20	0.23	1.2	0.52
12.575	$4f'[\frac{7}{2}]3, 4$	0.445						
12.575	$4f'[\frac{5}{2}]3$	0.445						
12.576	$4f'[\frac{5}{2}]2$	0.446						
12.576	$8s'[\frac{1}{2}]1$	0.446						
12.736	$8p'[\frac{3}{2}]1$	0.606	h	0.640	0.29	0.64	1.7	1.5
12.748	$8p'[\frac{1}{2}]1$	0.618						
12.749	$8p'[\frac{3}{2}]2$	0.619						
12.758*	$8p'[\frac{1}{2}]0$	0.628						
12.772*	$7d'[\frac{5}{2}]2$	0.642						
12.778*	$7d'[\frac{3}{2}]2$	0.648						
12.785*	$7d'[\frac{5}{2}]3$	0.655						
12.813	$7d'[\frac{3}{2}]1$	0.683	i	0.710	—	0.24	—	0.58
12.885	$9s'[\frac{1}{2}]0$	0.755	j	0.760	0.071	0.33	0.41	0.80
12.886	$5f'[\frac{7}{2}]3, 4$	0.756						
12.886	$5f'[\frac{5}{2}]2, 3$	0.756						
12.888	$9s'[\frac{1}{2}]1$	0.769						
12.980	$9p'[\frac{3}{2}](1), 2$	0.850	k	0.880	0.13	0.54	0.74	1.3
12.985	$9p'[\frac{1}{2}]0, (1)$	0.855						
12.991	$8d'[\frac{5}{2}]2$	0.861						
12.993	$8d'[\frac{3}{2}]2$	0.863						
12.998	$8d'[\frac{5}{2}]3$	0.868						
13.013	$8d'[\frac{3}{2}]1$	0.883						

Table 1. (Continued)

E (eV)	Level $n\ell'[K]J$	Ejected energy E_{ej} (eV)	TOF feature	TOF energy E_{ej} (eV)	R (%) 14 eV	R (%) 24 eV	σ ($\times 10^{-18}$ cm^2) 14 eV	σ ($\times 10^{-18}$ cm^2) 24 eV
13.054	$6f'[\frac{7}{2}]3, 4$	0.924						
13.054	$6f'[\frac{5}{2}]2, 3$	0.924						
13.055	$10s'[\frac{3}{2}]0$	0.925						
13.056	$10s'[\frac{3}{2}]1$	0.926						
13.111	$10p'[\frac{3}{2}](1), 2$	0.981						
13.114	$10p'[\frac{1}{2}]0, (1)$	0.984						
13.117*	$9d'[\frac{5}{2}]2$	0.987						
13.119	$9d'[\frac{3}{2}]1$	0.989						
13.121	$9d'[\frac{5}{2}]3$	0.991						
13.130	$9d'[\frac{3}{2}]1$	1.000						
13.156	$7f'[\frac{7}{2}]3, 4$	1.026						
13.156	$7f'[\frac{5}{2}]2, 3$	1.026	l					
13.157	$11s'[\frac{1}{2}]0, 1$	1.029						
13.193	$11p'[\frac{3}{2}](1), 2$	1.063						
13.195	$11p'[\frac{1}{2}]0, (1)$	1.065						
13.196	$10d'[\frac{5}{2}]2$	1.066						
13.197	$10d'[\frac{3}{2}]2$	1.067						
13.199	$10d'[\frac{5}{2}]3$	1.069						
13.205	$10d'[\frac{3}{2}]1$	1.075						
13.222	$8f'[\frac{7}{2}]3, 4$	1.092						
13.222	$8f'[\frac{5}{2}]2, 3$	1.092						
13.223	$12s'[\frac{1}{2}]0, 1$	1.093						
	⋮							
13.436	$Xe^{+}\,{}^2P_{1/2}$	1.306						
			Total		2.91	9.44	19	23

lifetime is so short. If an electron is ejected while the scattered electron is nearby, the ejected electron acquires extra kinetic energy since it is no longer escaping an ion, but a dipole.

There are six different unresolved levels which could contribute to feature g (see table 1). The optically allowed $8s'[\frac{1}{2}]1$ level probably contributes the most to the intensity at $E_0 = 24$ eV and above (figures 3 and 4) and while the optically forbidden $8s'[\frac{1}{2}]0$ and $4f'$ levels probably dominate at $E_0 = 14$ eV (figure 2). By plotting the energy shift of feature g as a function of current, it was observed that the shift had practically disappeared (to within a few meV) when extrapolating to zero current. The shift was not a linear function of current, but appeared to be reaching some asymptote with increasing current.

Feature h is made up of $8p'$ and $7d'$ levels which cannot be reached by an optically allowed transition from the ground state. Feature i is from the $7d'[\frac{3}{2}]1$ level, and appears to be shifted by 10 meV above its spectroscopic energy, but it is not clearly resolved. Feature j is due to overlapping $9s'$ and $5f'$ levels, feature k arises from $8d'$ and $9p'$ levels, and the last assigned feature is l (figure 4 only), from the $9d'[\frac{3}{2}]1$ and other levels. Higher up the

energy scale the remaining features overlap, forming a smooth continuum, until the abrupt drop at the $^2P_{1/2}$ ionic limit.

We have searched the literature and found only one other example of an ejected electron energy spectrum for Xe for the low AI levels. In that work (Penent *et al* 1990), Xe atoms were bombarded by H^- ions at 5 keV. A 127° cylindrical analyser was used to obtain an ejected electron spectrum which closely resembles ours, except the features which lie below 0.4 eV do not appear in their spectra. It may be possible that PCI with H^- ions has something to do with this, but it is more likely that it was caused by an instrumental effect in their energy analyser since, as stated earlier, it becomes increasingly difficult to collect, focus, and analyse electrons as their kinetic energy decreases. This illustrates one advantage of using TOF electron spectroscopy over conventional electrostatic EELS.

Another advantage of TOF spectroscopy is that a direct comparison of the intensity of two different features in a TOF spectrum can be made without factoring in the instrumental collection efficiency, as is done with conventional electrostatic electron energy analysers. Thus, it is possible to calculate the electron scattering differential cross section (DCS) for one feature, by means of comparison with another feature for which the DCS is known. This has been discussed in our previous paper (LeClair and Trajmar 1996) and can be briefly described as follows. First, the intensity of the elastic feature is used since elastic DCS's are well established, and the elastic feature in TOF spectra is usually well separated from other features. The scattering intensity associated with the elastic feature (I_{el}) is related to the elastic DCS by the following proportionality:

$$I_{el}(E_0, \theta) \propto \int j(x, y, z) n(x, y, z) \mathrm{DCS}_{el}(E_0, \theta) \Delta\Omega(x, y, z)\, \mathrm{d}V, \tag{4}$$

where j is the current density; n is the number density of gas molecules which make up the target; DCS_{el} is the elastic differential cross section at E_0 and θ; $\Delta\Omega$ is the view cone into which the scattered electrons are collected; and $\mathrm{d}V$ is the volume element located at position (x, y, z). The scattering intensity associated with an inelastic feature (I_{inel}) is related to the inelastic DCS by the same proportionality, equation (4), except DCS_{el} is replaced by DCS_{inel}. By taking a ratio of the two proportionalities one obtains $\mathrm{DCS}_{inel} = \mathrm{DCS}_{el} I_{inel}/I_{el}$ for a given E_0 and θ.

For electron impact excitation of autoionizing levels this method cannot be applied since, as stated earlier, the scattered electrons causing excitation of individual autoionizing levels cannot be resolved in the present TOF spectra. Thus, the DCS for scattering from those levels cannot be determined. However, it is possible to obtain a reasonable estimate of the integral cross section for electron impact excitation of an autoionizing level by a comparison between the intensity of features due to elastically scattered electrons and ejected electrons. This estimate requires two assumptions. First, *it is assumed that the ejected electrons are emitted isotropically*. We have no means to test this assumption with the present apparatus. It certainly cannot hold if PCI takes place. Secondly, the autoionizing features in the kinetic energy spectra are not peaks but Beutler–Fano profiles superposed on a background of electrons associated with the $^2P_{3/2}$ continuum. Beutler–Fano profiles typically have a portion which extends above the continuum and one which extends below. *It is assumed that the negative going portion of the Beutler–Fano profile is very small* since we see no evidence of it in the kinetic energy spectra. Thus the features can be treated as peaks on a background and their intensities can be easily determined. The intensity of an ejected-electron feature (I_{AI}) is then related by the following proportionality:

$$I_{AI}(E_0) \propto \int j(x, y, z) n(x, y, z) \sigma_{AI}(E_0) \Delta\Omega(x, y, z)\, \mathrm{d}V/(4\pi), \tag{5}$$

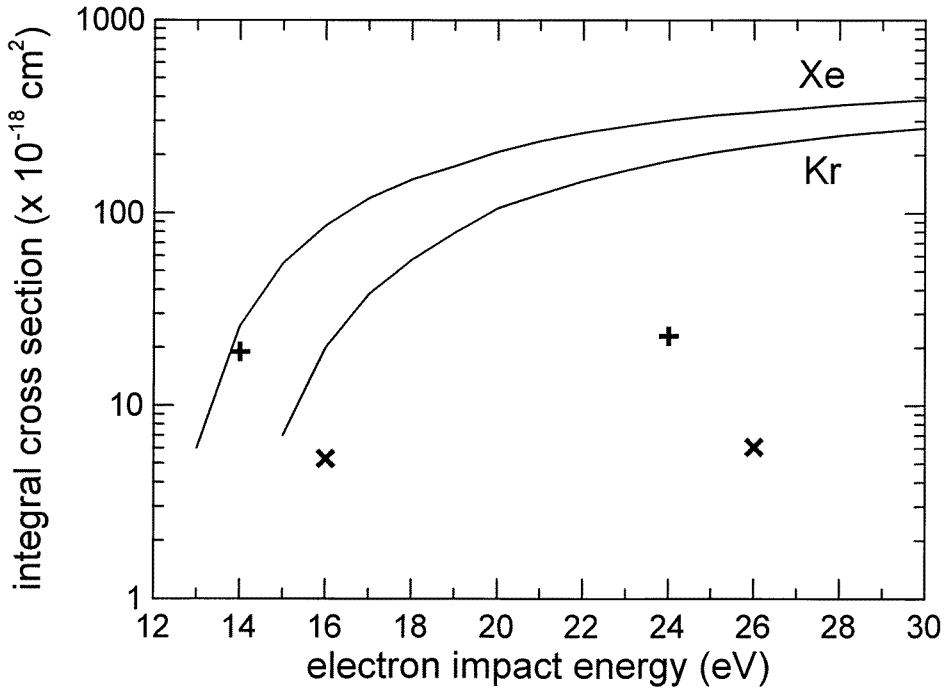

Figure 5. The total integral cross section for electron impact ionization of Kr and Xe (full curves), interpolated from the data of Krishnakumar and Srivastava (1988). Also shown are the integral cross sections for autoionization by all levels between the $^2P_{3/2}$ and $^2P_{1/2}$ ionic limits of Kr (×) and Xe (+) as determined from the TOF spectra.

where σ_{AI} is the integral cross section for electron-impact excitation of an autoionizing level. Dividing (5) by (4) we obtain

$$\sigma_{AI} = 4\pi R \mathrm{DCS}_{el}(E_0, \theta) \tag{6}$$

where $R = I_{AI}/I_{el}$, the ratio of the intensities obtained from the TOF spectra.

Equation (6) was applied to most features in figures 2 and 3 and the results for R and σ appear in table 1. The values for $\mathrm{DCS}_{el}(\theta = 90°)$ for Xe at 14 and 24 eV were obtained by interpolation of the experimental data of Register *et al* (1986) (46 and 19×10^{-18} cm^2 sr^{-1} respectively, ±30%). The errors in calculating R are estimated to be between 25% and 75% because of the overlap between features which required unfolding, and the uncertainty in the background. For the background, we fitted two exponentials to trace out the minima which appear between features a–k in the TOF spectra. An example is shown in figure 1. By subtracting this reasonable estimate for the background, we were also able to obtain the total autoionization intensity and calculate the integral cross sections for autoionization by all levels between the ionic limits for impact energies of 14 and 24 eV. These are plotted in figure 5 along with the integral cross section for electron impact ionization of Xe as measured by Krishnakumar and Srivastava (1988). At 14 eV, electron impact ionization by means of autoionization accounts for about two-thirds of the ionization cross section, and this drops to about 7.5% at 24 eV.

Note that in equation (6) we are comparing the intensities which come from low-energy electrons (< 1 eV) with those of higher energy (by more than a factor of 10). We cannot say for certain that all of the low-energy electrons are being collected as efficiently as

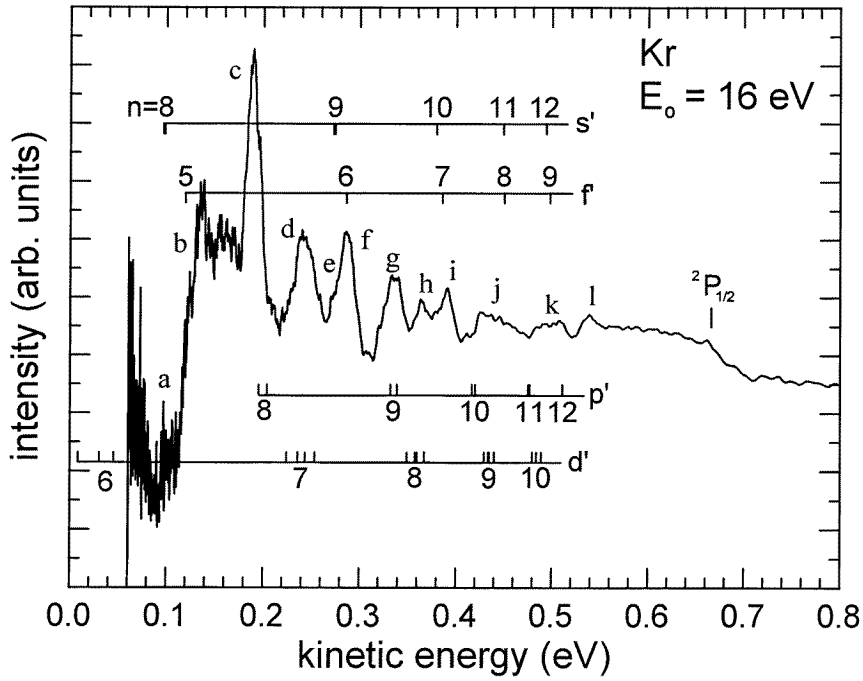

Figure 6. Same as in figure 2, but for Kr at $E_0 = 16$ eV. The letters assigned to the features from Kr are not related to the letters assigned to the features from Xe.

the higher-energy electrons, owing to patch fields, etc, and so our cross sections must be considered an estimate, and possibly a lower-bound estimate.

3.2. Kr

Kinetic energy spectra of electrons ejected from the low autoionizing levels of Kr are shown in figures 6 and 7 for $E_0 = 16$ and 26 eV, respectively. They were both obtained using 10 nA of electron current. Due to a lack of time and a change of research interests we were not able to obtain spectra at higher current and electron-impact energy. The features are labelled a–l and identified in table 2. The energies which are listed in table 2 came from spectroscopic measurements by Delsart and Keller (1983), Wada *et al* (1987), Klar *et al* (1992), Maeda *et al* (1993), and Koeckhoven *et al* (1994, 1995). Wada *et al* (1987) obtained measurements for the 7d′ levels only. Since there are no measurements of the energies of the remaining members of the nd′ series, those energies were calculated from the quantum defects for the 7d′ levels, except for the optically allowed nd′[$\frac{3}{2}$]1 levels for which accurate measurements exist (Maeda *et al* 1993).

The Kr data were acquired following our work with Xe. Surface patch fields had increased such that the kinetic energy spectra from Kr had to be shifted by about 25 meV in order to identify the features. This was determined by shifting the kinetic energy spectrum taken at $E_0 = 26$ eV so that features a and e matched the spectroscopic energies of the 8s′[$\frac{1}{2}$]1 and 7d′[$\frac{3}{2}$]1 levels, respectively. Both features a and e are absent from the spectrum taken at 16 eV, hence they must be associated with levels which arise from optically allowed transitions. The 25 meV shift resulted in a good match between the remaining features and

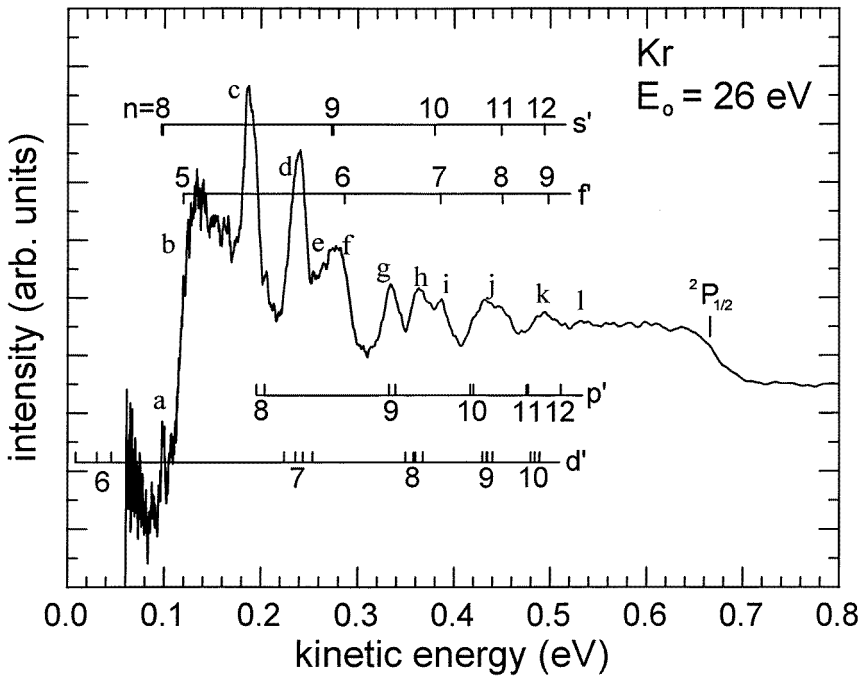

Figure 7. Same as in figure 6, but $E_0 = 26$ eV.

their spectroscopically determined energies.

As with the kinetic energy spectrum obtained from Xe, there is a sharp drop in intensity in figures 6 and 7 below 0.1 eV which is attributed to patch fields in the drift tube. This leads to a greatly diminished intensity for feature a (compared to Xe). Feature a appears to be indiscernible from the noise which surrounds it, but it does appear in the TOF spectrum as a small bump at 1340 ns. The width of feature a is approximately 5 meV. To the left of feature a one can see what appears to be structure from the 6d′ terms, but we could not discern anything from the background in the TOF spectra in that range (over 1500 ns). Feature b appears to be due to the 5f′ terms; some structure can be discerned at 16 eV, but little else at 26 eV, possibly due to the distortion from the patch fields.

Feature c can probably be associated with the 8p′ term, even though it is slightly lower in energy than spectroscopic measurements, since half of the fine structure levels of the 8p′ term have not yet been measured. Feature d arises from the unresolved 7d′[$\frac{5}{2}$]2, 7d′[$\frac{5}{2}$]3, and 7d′[$\frac{3}{2}$]2 terms. As in the case with Xe, both the np′ and nd′ autoionizing series are very intense at these impact energies. As stated earlier, feature e arises from the optically allowed 7d′[$\frac{3}{2}$]1 level, and feature f from the 9s′ and 6f′ terms. Features g, h, and i are simply the next higher members of the levels which contributed to features c, d, e, and f. Likewise, feature j is made up of the next higher members of the levels in features g, h, and i, but they are unresolved. Similar assignments apply to features k and l.

The ratios and calculated integral cross sections associated with some of the features are compiled in table 2, along with the summed cross sections for all the low AI levels in Kr. The values for $\mathrm{DCS}_{el}(\theta = 90^\circ)$ for Kr at 16 and 26 eV were obtained by interpolation of the experimental data of Danjo (1988) (40 and 24×10^{-18} cm^2 sr^{-1} respectively, $\pm 20\%$). The total low AI level cross sections have also been plotted in figure 5 for comparison with

Table 2. Same as table 1, but for Kr, with $E_0 = 16$ and 26 eV. The ionization potentials used for $Kr^+[^2P_{3/2}]$ and $Kr^+[^2P_{1/2}]$ were 14.000 eV and 14.665 eV, respectively (Bounakhla *et al* 1993). The spectroscopic energies for the first column were obtained from the measurements of Delsart and Keller (1983), Wada *et al* (1987), Klar *et al* (1992), Maeda *et al* (1993), and Koeckhoeven *et al* (1994, 1995).

E (eV)	Level $n\ell'[K]J$	Ejected energy E_{ej} (eV)	TOF feature	TOF energy E_{ej} (eV)	R (%) 16 eV	R (%) 26 eV	σ ($\times 10^{-18}$ cm^2) 16 eV	σ ($\times 10^{-18}$ cm^2) 26 eV
14.009*	6d′[$\frac{5}{2}$]2	0.009	—	—	—	—	—	—
14.032*	6d′[$\frac{3}{2}$]2	0.032	—	—	—	—	—	—
14.044*	6d′[$\frac{5}{2}$]3	0.044	—	—	—	—	—	—
14.070	6d′[$\frac{3}{2}$]1	0.070	—	—	—	—	—	—
15.097	8s′[$\frac{1}{2}$]0	0.097	a	0.100	—	—	—	—
14.099	8s′[$\frac{1}{2}$]1	0.099						
14.118	5f′[$\frac{7}{2}$]4, (3)	0.118	b	0.130	—	—	—	—
14.119	5f′[$\frac{5}{2}$]2, (3)	0.119						
14.196	8p′[$\frac{3}{2}$]2, (1)	0.196	c	0.190	0.075	0.11	0.38	0.34
14.204	8p′[$\frac{1}{2}$]0, (1)	0.204						
14.224	7d′[$\frac{5}{2}$]2	0.224	d	0.240	0.090	0.10	0.45	0.31
14.237	7d′[$\frac{3}{2}$]2	0.237						
14.244	7d′[$\frac{5}{2}$]3	0.244						
14.258	7d′[$\frac{3}{2}$]1	0.258	e	—	—	0.051	—	0.15
14.274	9s′[$\frac{1}{2}$]0	0.274	f	0.275	0.074	0.10	0.38	0.31
14.275	9s′[$\frac{1}{2}$]1	0.275						
14.287	6f′[$\frac{7}{2}$]4, (3)	0.286						
14.287	6f′[$\frac{5}{2}$]2, (3)	0.287						
14.332	9p′[$\frac{3}{2}$]2, (1)	0.332	g	0.335	0.063	0.086	0.32	0.26
14.338	9p′[$\frac{1}{2}$]0, (1)	0.338						
14.349*	8d′[$\frac{5}{2}$]2	0.349	h	0.360	0.033	0.079	0.17	0.24
14.357*	8d′[$\frac{3}{2}$]2	0.357						
14.360*	8d′[$\frac{5}{2}$]3	0.360						
14.369	8d′[$\frac{3}{2}$]1	0.369						
14.380	10s′[$\frac{1}{2}$]0, 1	0.380	i	0.385	0.042	0.066	0.21	0.20
14.387	7f′[$\frac{7}{2}$]4, (3)	0.387						
14.387	7f′[$\frac{5}{2}$]2, (3)	0.387						
14.417	10p′[$\frac{3}{2}$]2, (1)	0.417	j	0.440	—	0.12	—	0.35
14.420	10p′[$\frac{1}{2}$]0, (1)	0.420						
14.427*	9d′[$\frac{5}{2}$]2	0.427						
14.432*	9d′[$\frac{3}{2}$]2	0.432						
14.435*	9d′[$\frac{5}{2}$]3	0.435						
14.440	9d′[$\frac{3}{2}$]1	0.440						
14.448	11s′[$\frac{1}{2}$]0, 1	0.448						
14.453	8f′[$\frac{7}{2}$]4, (3)	0.453						
14.453	8f′[$\frac{5}{2}$]2, (3)	0.453						

Table 2. (Continued)

E (eV)	Level $n\ell'[K]J$	Ejected energy E_{ej} (eV)	TOF feature	TOF energy E_{ej} (eV)	R (%) 16 eV	R (%) 26 eV	σ ($\times 10^{-18}$ cm^2) 16 eV	σ ($\times 10^{-18}$ cm^2) 26 eV
14.473	$11p'[\frac{3}{2}](1), 2$	0.473						
14.475	$11p'[\frac{1}{2}]0, (1)$	0.475						
14.480*	$10d'[\frac{5}{2}]2$	0.480						
14.483*	$10d'[\frac{3}{2}]2$	0.483						
14.485*	$10d'[\frac{5}{2}]3$	0.485						
14.488	$10d'[\frac{3}{2}]1, (2)$	0.488	k	0.490				
14.494	$12s'[\frac{1}{2}]0, 1$	0.494						
14.498	$9f'[\frac{7}{2}]4, (3)$	0.498						
14.498	$9f'[\frac{5}{2}]2, (3)$	0.498						
14.512	$12p'[\frac{3}{2}](1), 2$	0.512						
14.513	$12p'[\frac{1}{2}]0, (1)$	0.513						
14.516*	$11d'[\frac{5}{2}]2$	0.516						
14.519*	$11d[\frac{3}{2}]2$	0.519						
14.520*	$11d'[\frac{5}{2}]3$	0.520						
14.523	$11d'[\frac{3}{2}]1$	0.523	l	0.540				
14.527	$13s'[\frac{1}{2}]0, 1$	0.527						
14.530	$10f'[\frac{7}{2}]4, (3)$	0.530						
14.530	$10f'[\frac{5}{2}]2, (3)$	0.530						
	⋮							
14.665	$Kr^+\ ^2P_{1/2}$ limit	0.665						
			Total		1.05	2.02	5.3	6.1

the total ionization cross section of Kr by electron impact as measured by Krishnakumar and Srivastava (1988). The results are similar to those obtained from Xe, except that the fraction of the total ionization cross section due to autoionization is smaller.

4. Conclusion

Kinetic energy spectra of electrons ejected from autoionizing levels of Kr and Xe which lie between the $^2P_{3/2}$ and $^2P_{1/2}$ ionic limits have been obtained using field-free TOF electron spectroscopy. An attempt was made to obtain the same from Ar, but no features could be resolved. For Kr and Xe it was possible to see distinct features due to AI from particular energy levels, and to produce a reasonable estimate of the electron-impact excitation integral cross sections for these levels, with certain assumptions. The assumption that the ejected electrons are emitted isotropically could not be checked since the drift tube was fixed at 90°, and the angle could not be changed without substantial redesign and construction. We were also not able to test how well the assumption holds for levels with different AI lifetimes, or with respect to the amount of incident electron current. It would be interesting to continue this work, but not on the present apparatus. First, the pulse width of the electron gun would have to be shortened in order to improve the resolution of the autoionization features. Secondly, and more importantly, our vacuum system cannot maintain the necessary

cleanliness required for the length of time it would take to do a thorough study. Patch fields attenuated features below 0.1 eV. After two weeks of operation this cut-off would increase, low kinetic energy AI features would diminish in intensity or disappear, and higher-energy features would shift dramatically, indicating contamination of the surfaces exposed to the electrons. However, for the time being, the presence of sharp features in the kinetic energy spectra with energies of about 0.1–0.2 eV represents a benchmark in EELS, and the measurement of AI excitation cross sections appears to be novel as well.

Acknowledgments

This work was carried out at the Jet Propulsion Laboratory, California Institute of Technology, under contract with the National Aeronautics and Space Administration. The authors wish to thank M A Khakoo for providing the design and construction of the electron gun. One of us (LRL) is grateful to the NRC for being awarded a Resident Research Associateship. We would also like to thank S M Koeckhoven, W J Buma and C A de Lange for useful information.

References

Baxter J A, Mitchell P and Comer J 1983 *J. Phys. B: At. Mol. Phys.* **15** 1105
Bounakhla M, Lemoigne J P, Grandin J P, Husson X, Kucal H and Aymar M 1993 *J. Phys. B: At. Mol. Opt. Phys.* **26** 345
Comer J 1992 *Aust. J. Phys.* **45** 309
Danjo A 1988 *J. Phys. B: At. Mol. Opt. Phys.* **21** 3759
Delsart C and Keller J-C 1983 *Phys. Rev.* A **28** 845
Grandin J-P and Husson X 1981 *J. Phys. B: At. Mol. Phys.* **14** 433
Hammond P, Read F H and King G C 1988 *J. Phys. B: At. Mol. Opt. Phys.* **21** 3123
Hildebrand F B 1987 *Introduction to Numerical Analysis* (New York: Dover) ch 7
Inokuti M 1971 *Rev. Mod. Phys.* **43** 297
Klar D, Harth K, Ganz J, Kraft T, Ruf M-W, Hotop H, Tsemekhman V, Tsemekhman K and Amusia M Ya 1992 *Z. Phys.* D **23** 101
Koeckhoven S M, Buma W J and de Lange C A 1994 *Phys. Rev.* A **49** 3322
——1995 *Phys. Rev.* A **51** 1097
Krishnakumar E and Srivastava S K 1988 *J. Phys. B: At. Mol. Opt. Phys.* **21** 1055
LeClair L R and Trajmar S 1996 *J. Phys. B: At. Mol. Opt. Phys.* **29** 5543–66
LeClair L R, Trajmar S, Khakoo M and Nickel J 1996 *Rev. Sci. Instrum.* **67** 1753
Maeda K, Ueda K and Ito K 1993 *J. Phys. B: At. Mol. Opt. Phys.* **26** 1541
Marmet P and Proulx M 1990 *J. Phys. B: At. Mol. Opt. Phys.* **23** 549
Moore C E 1957 *Atomic Energy Levels* NSRDS-NBS Publication 35 vol 3 (Washington, DC: US Govt Printing Office)
Penent F, Grouard J P, Montmagnon J L and Hall R I 1990 *J. Phys. B: At. Mol. Opt. Phys.* **23** L449
Read F H and Hammond P 1988 *J. Phys. B: At. Mol. Opt. Phys.* **21** 4225
Register D F, Vušković L and Trajmar S 1986 *J. Phys. B: At. Mol. Phys.* **19** 1685
Wada A, Adachi Y and Hirose C 1987 *J. Chem. Phys.* **86** 5904
Wang L and Knight R D 1986 *Phys. Rev.* A **34** 3902